# On the structure of high performance anticorrosive PMMA–siloxane–silica hybrid coatings

**Article** *in* RSC Advances · December 2015

DOI: 10.1039/C5RA20885H



**7 authors**, including:

Fábio Cesar
São Paulo State University
**6** PUBLICATIONS **110** CITATIONS
SEE PROFILE

Samarah Vargas Harb
Universidade Federal de São Carlos
**13** PUBLICATIONS **54** CITATIONS
SEE PROFILE

Marie-Joëlle Menu
Paul Sabatier University - Toulouse III
**60** PUBLICATIONS **856** CITATIONS
SEE PROFILE

Viviane Turq
Paul Sabatier University - Toulouse III
**38** PUBLICATIONS **579** CITATIONS
SEE PROFILE

RSC Advances

PAPER

View Article Online
View Journal | View Issue



Cite this: *RSC Adv.*, 2015, **5**, 106754

# On the structure of high performance anticorrosive PMMA–siloxane–silica hybrid coatings†

Fábio C. dos Santos,[a] Samarah V. Harb,[a] Marie-Joëlle Menu,[b] Viviane Turq,[b] Sandra H. Pulcinelli,[a] Celso V. Santilli[a] and Peter Hammer*[a]

Received 9th October 2015
Accepted 4th December 2015

DOI: 10.1039/c5ra20885h

www.rsc.org/advances

Environmentally compliant organic–inorganic hybrid coatings for efficient corrosion protection of metallic surfaces are potential alternatives to the current method based on chromate passivation. In this context PMMA–siloxane–silica (PMMA–SS) hybrid films were prepared using the sol–gel process from the radical copolymerization of methyl methacrylate and 3-(trimethoxysilyl)propyl methacrylate followed by acidic hydrolysis and polycondensation of tetraethoxysilane (TEOS), under variation of the ethanol to $H_2O$ ratio (0.0–1.0). The structural properties of about 2 μm thick coatings, deposited by dip-coating onto carbon steel, were related with their corrosion protection efficiency. The correlation of data obtained by X-ray photoelectron spectroscopy, nuclear magnetic resonance and small angle X-ray scattering has shown for intermediate ethanol to $H_2O$ ratios the highest connectivity (~83%) of the inorganic phase, bonded covalently to organic moieties, yielding a dense and homogeneous nanocomposite structure with high thermal stability, very good adhesion to the metallic substrate and excellent barrier properties. The electrochemical impedance spectroscopy measurements have shown for coatings prepared at intermediate EtOH/$H_2O$ ratios a high corrosion resistance of almost 10 GΩ cm$^2$, which remained unchanged for more than 6 months in contact with 3.5% NaCl solution and more than 3 months exposed to an acidic NaCl environment.



## Introduction

Organic–inorganic hybrid nanocomposites stand for a class of materials, which combine components with different characteristics, resulting in a system that does not represent only the sum of properties of the individual parts, but a new material with unique features. The blend of organic and inorganic phases, linked on the molecular scale, combines properties like processability, flexibility and hydrophobicity of the polymeric compounds with thermal, chemical and mechanical stability of ceramic materials. The high flexibility of the sol–gel process in terms of variability of the nature and proportion of precursors, including specific dopants, results in hybrid nanocomposites with tunable properties, allowing their application in drug delivery systems, optical and electrical devices, catalysis, photochromic systems, protective coatings, *etc.*[1,2] The conventional synthesis of this multifunctional material is based on the hydrolytic condensation of the inorganic phase, together with the polymerization of the organic precursor, resulting in physical interaction and/or chemical bonding between both constituents. In the latter case, the introduction of a coupling agent, leads to the formation of class II hybrid presenting covalent bonds between organic and inorganic component.[1,3]

More specifically, the combination of polymethyl methacrylate (PMMA) with silica backbone leads to the inclusion of the polymeric phase into the pores of the inorganic network, resulting in a dense material, suitable for corrosion protection application. Recent studies have shown that protective coatings, based on PMMA–siloxane–silica hybrids (PMMA–SS), are excellent candidates for an efficient and environmentally compliant protection of metallic surfaces.[4,5] This is related to the highly cross-linked inorganic structure, which harbors the polymeric phase, thus providing elevated thermal and mechanical stability and excellent adhesion to metallic substrates. The PMMA phase, covalently bonded to the silica network hermetically seals the structure and provides a hydrophobic character to the coating, blocking the diffusion of corrosive agents, thus preserving the integrity of the metallic substrate.[5,6]

Especially in the case of exposure to a medium containing chloride, the corrosion resistance of the metallic surface is strongly affected, with a tendency to suffer generalized corrosion. The consequence is the loss of aesthetic appearance and structural integrity, leading to problems with safety and high costs for the substitution of damaged parts.[7,8] In the aviation industry and many household appliances, where aluminum and different ferrous alloys are largely used, the common based

[a]*Instituto de Química, UNESP-Univ Estadual Paulista, 14800-060 Araraquara, SP, Brazil. E-mail: peter@iq.unesp.br; Tel: +55 16 3301 9887*

[b]*Université Paul Sabatier - Toulouse III, 31062 Toulouse Cedex 9, France*

† Electronic supplementary information (ESI) available. See DOI: 10.1039/c5ra20885h

passivation method is still the application of chromates, involving harmful hexavalent chromium species. In this context, organic–inorganic hybrid coatings have a great potential to serve as environmentally correct substitutes for chromate, providing a long-term protection of various metal alloys (steel, aluminum, magnesium, *etc.*) used in aerospace, automotive and offshore industries. In addition to their excellent corrosion protection efficiency, other aspects favor the use of organic–inorganic hybrids, among which should be highlight the mild synthesis conditions provided by the sol–gel method, the low costs of production, environmental compatibility and the low temperatures needed to cure the coatings.[4,9]

Considering the great potential of PMMA–SS hybrids as protective coatings, this work focuses on the investigation of the sol–gel synthesis parameters on the formation of the hybrid network. A better understanding of the effect and interplay of different preparation conditions on the formation of the hybrid network is crucial for a further improvement of the barrier properties of the material. After establishing in a previous study the best proportion between the polymeric and silica phase yielding for the MMA to TEOS ratio of 4 a highly ramified hybrid network, this paper focuses on a further improvement of the structure by a careful adjustment of the sol–gel conditions in direct feedback to detailed structural results obtained by a number of complementary characterization techniques.[5] One important parameter is the ethanol to water ratio ($EtOH/H_2O$), which controls the kinetics of the hydrolysis and condensation reactions, taking place during the formation of the inorganic phase. The aim of this work was to determine the best conditions for the formation of highly cross-linked silica nodes, covalently interconnected with short polymeric chains, providing a high overall connectivity of the hybrid network. This was achieved by correlating structural data obtained from X-ray photoelectron spectroscopy (XPS), $^{29}Si$ nuclear magnetic resonance (NMR), small angle X-ray scattering (SAXS), with results obtained from mechanical and electrochemical measurements. The corrosion protection efficiency was investigated by electrochemical impedance spectroscopy (EIS) after long-term immersion in acidic and neutral saline solution. The mechanical properties of the coatings were investigated by scratch tests and nanoindentation, while the surface morphology was studied using atomic force microscopy (AFM).

## Experimental

Following commercially available reagents were used as received: tetraethylorthosilicate (TEOS, Sigma-Aldrich), 3-(trimethoxysilyl)propyl methacrylate (MPTS, also known as TMSM, Sigma-Aldrich), ethanol (Sigma-Aldrich), tetrahydrofuran (THF, Sigma-Aldrich), nitric acid (Sigma-Aldrich) and benzoyl peroxide (BPO, Sigma-Aldrich). The methyl methacrylate (MMA, Sigma-Aldrich) was distillated to remove the inhibitor of polymerization. The polymethyl methacrylate–siloxane–silica samples were prepared using the sol–gel route in following sequence: first the MMA and the coupling agent (MPTS) were polymerized in THF using the thermal initiator (BPO) during 2 h at 70 °C under magnetic stirring. Then, the inorganic component of the hybrid was prepared by hydrolysis and condensation of silicon alkoxide (TEOS). The hydrolysis of TEOS was carried out in ethanol solution by addition of acidified water (pH = 1) using nitric acid. After 1 h of stirring at 25 °C in a closed flask, the suspension was mixed with the polymer solution forming a homogeneous and transparent sol used for film deposition. Considered as the most suitable precursor ratio for the synthesis of corrosion protection coating, the MMA to TEOS molar ratio of 4 (reference sample M4) was kept constant. The ethanol to $H_2O$ proportions were 0.0, 0.1, 0.2, 0.5, 0.7 and 1.0, denoting the samples as M4E00, M4E01, M4E02, M4E05, M4E07 and M4E1. All other ratios were kept constant: $H_2O/Si = 3.5$, BPO/MMA = 0.01 and TEOS/MPTS = 2.0.[5]

For EIS, AFM, scratch test, nanoindentation, adhesion, XPS and thickness measurements, coated A1010 carbon steel substrates (25 mm × 25 mm × 4 mm) were used, having a nominal composition (wt%) of C = 0.08–0.13%, Mn = 0.3–0.6%, P = 0.04% and S = 0.05%, with the balance of Fe. The deposition of hybrid coatings was performed by dip-coating, applying 3 dips at a withdraw rate of 14 cm $min^{-1}$. For SAXS and TG analysis unsupported films were prepared on Teflon support. The coated substrates and unsupported hybrids were annealed at 60 °C for 24 h and finally cured at 160 °C during 3 h which ensured a complete polymerization of the hybrid structure.[4] For NMR measurements the dried unsupported films were milled to powder.

The coatings thickness was determined using Filmetrics F3-CS optical interference system. The adhesion of the films to the steel surface was evaluated by the ASTM D4541 method using a Posi-Test Pull-Off Adhesion Tester (De Felsko), determining the tensile pull-off force of detaching. AFM measurements were carried out using the tapping mode of the Agilent 5500 instrument. The topography images (0.3 × 0.3 $\mu m^2$) were used to obtain the coating surface roughness.

Scratch tests were performed using a scratch tester (CSM) with a diamond tip (2 μm) with conical/spherical geometry. The tests were carried out on a track of 1 mm with progressive loading from 0.3 to 100 mN to evaluate scratch resistance and adherence of the coatings. During the scratch test different stages of deformation and the corresponding critical loads were determined from optical microscopy images. Nanoindentation were conducted using an ultra-nanoindentation tester (CSM) with maximum force of 500 mN in 4 different regions, contact time of 60 s and a penetration depth of about 200 nm.

$^{29}Si$ and $^{13}C$ magic-angle spinning nuclear magnetic resonance (MAS-NMR) spectra were recorded using a VARIAN spectrometer operating at 300 MHz and 7.05 T. The Larmor frequency was 59.59 Hz and 75.42 Hz for $^{29}Si$ and $^{13}C$, respectively. The spectra were obtained from the Fourier transformation of the free induction decays (FID), following a single $\pi/2$ excitation pulse and a dead time of 2 s. Chemical shifts were referenced to tetramethylsilane (TMS), used as external standard. The $^{13}C$ spectrum of MMA was obtained in liquid state, using chloroform ($CDCl_3$) as solvent, to compare the chemical shifts. The uncertainty in the chemical shift values was estimated to be less than 0.5 ppm.

The SAXS measurements of unsupported hybrid films were performed using the SAXS 2 beam-line at the National Synchrotron Light Laboratory (LNLS) in Campinas, Brazil. An asymmetrically cut and bent Si(111) crystal was used to focus horizontally the monochromatic X-ray beam ($\lambda = 0.1608$ nm). The scattering intensity $I(\boldsymbol{q})$, collected with a two-dimensional X-ray detector (Pilatus, 300k, 84 mm × 107 mm), was determined as a function of the modulus of the scattering wave vector $\boldsymbol{q} = 4\pi/\lambda \sin\theta$, $\theta$ being half of the scattering angle. With sample-to-detector distance fixed at 0.8 m, the scattering vector, $\boldsymbol{q}$, was varied between 0.2 and 4.8 $nm^{-1}$. The parasitic scattering was subtracted from the total scattering intensity. The resulting curves were corrected to account for the effects related to the detector sensitivity and sample transmission.

The TG curves of samples were recorded using a SDT Q600 (TA Instruments) thermal analysis system, with nitrogen as purge gas at a flow rate of 100 mL $min^{-1}$. About 7 mg of the unsupported films were heated in alumina crucibles at a rate of 10 °C $min^{-1}$ up to 600 °C.

The XPS analysis was carried out at a pressure of less than $10^{-7}$ Pa using a UNI-SPECS UHV instrument. The Mg Kα line was used ($h\nu = 1253.6$ eV) and the analyzer pass energy for the high-resolution spectra was set to 10 eV. The inelastic background of the C 1s, O 1s and Si 2p spectra was subtracted using Shirley's method. Due to sample charging, the binding energy scale was corrected using ester component of PMMA (C 1s) fixed at 288.8 eV. The composition was determined with an accuracy of ±10% from the ratio of the relative peak areas corrected sensitivity factors of the corresponding elements. The spectra were fitted without placing constraints using multiple Voigt profiles. The width at half maximum (FWHM) varied between 1.2 and 2.1 eV and the accuracy of the peak positions was ±0.05 eV. To guaranty a consistent interpretation of structural and electrochemical data, XPS analysis was performed also on unsupported films, used for NMR, SAXS and TG, and coated carbon steel. The obtained results confirmed the identity of both materials.

The electrochemical measurements of the bare and coated carbon steel samples were carried out for different immersion periods at 25 °C in 80 mL of naturally aerated and unstirred 0.05 mol $L^{-1}$ $H_2SO_4$ + 0.05 mol $L^{-1}$ NaCl aqueous solution and in neutral 3.5% NaCl aqueous solution. For impedance measurements an Ag/AgCl/$KCl_{sat}$ electrode, connected to the working solution through a Luggin capillary, was used as reference, and a Pt grid as the auxiliary electrode. To minimize high-frequency phase shifts in impedance measurements, a fourth Pt electrode was connected to the reference electrode through a 0.1 μF capacitor. The working electrode was mounted in an electrochemical flat cell, exposing a geometric area of 1 $cm^2$ to the solution. The EIS measurements were performed after different immersion periods in saline and saline/acidic solutions using a potentiostat/galvanostat EG&G Parc-273A and a frequency response analyzer Solartron-SI 1260. The EIS tests were performed applying 10 mV (rms) to the open circuit potential ($E_{OC}$) value, starting from $10^4$ to $10^{-2}$ Hz with 10 points per decade. For all samples, $E_{OC}$ was measured for 15 min and then the impedance spectra recorded. To guarantee the reproducibility of the results all electrochemical measurements were performed in duplicate.

## Results and discussion

### Structural features

Using the sol–gel process PMMA–SS hybrids were prepared by the simultaneous hydrolytic condensation of the inorganic phase and the polymerization of organic species. As the hydrolysis and condensation process of TEOS liberates ethanol, the initial EtOH/$H_2O$ ratio is an important phase formation factor, which influences kinetics of the well-known hydrolysis and condensation reactions (ESI, Scheme S1†). Consequently, the addition of alcohol in the hydrolysis reaction shifts the chemical equilibrium in the opposite direction of the reactions (ESI, eqn (1) of Scheme S1†). On the other hand, TEOS and water form a biphasic system (polar and nonpolar) and the addition of small volumes of ethanol acts as co-solvent favoring the homogenization of water (polar) and TEOS (nonpolar) mixture and the formation of a single liquid phase. Therefore, it is expected that ethanol acts as a dispersion agent enhancing the uniformity of distribution of silicon species into the continuous liquid phase.[10]

To investigate polymerization degree of the organic phase of the hybrids nanocomposites the $^{13}C$ solid state magic-angle spinning nuclear magnetic resonance (MAS-NMR) was applied, (Fig. 1a). The comparison of the resonance signals of the MMA reference with those obtained for M4E00, M4E05 and M4E1 samples indicates a complete polymerization of the organic phase. The shift of the peaks b → b′ and a → a′ to lower ppm values evidenced the formation of a quaternary carbon atom and an aliphatic $CH_2$ group, respectively, caused by the loss of the vinylic double bond.[11] Another consequence is the small up-shift of the ester (c → c′) and –$CH_3$ groups (d → d′ and e → e′). The aliphatic C–Si, $CH_2$ and C–O groups of MPTS are located at about 12 ppm, 28 ppm and 60 ppm, respectively,[5] and the signal at 117 ppm (•) is related to a spinning side band.[12]

The connectivity of the silica network was studied using $^{29}Si$ MAS-NMR. Fig. 1b displays the $^{29}Si$ NMR spectra of hybrid samples prepared using different EtOH/$H_2O$ ratios (0.0, 0.5 and 1.0). The observed broad resonances at −48.5, −57.5 and −65.0 ppm were assigned to $T^1$ (–$CH_2Si(OSi)(OR)_2$, R = H or $CH_3$), $T^2$ (–$CH_2Si(OSi)_2(OR)$) and $T^3$ (–$CH_2Si(OSi)_3$) structural units, respectively, related to the polycondensation product of MPTS.[12] Resonances related to TEOS polycondensation products were detected at −92.3, −101.0 and −109.5 ppm, corresponding to $Q^2$ ($Si(OSi)_2(OR)_2$, R = H or $CH_2CH_3$), $Q^3$ ($Si(OSi)_3(OR)$) and $Q^4$ ($Si(OSi)_4$) species, respectively.[13] The absence of monomer species $T^0$ (–$CH_2Si(OR)_3$) and $Q^0$ ($Si(OR)_4$) is in agreement with the cluster–cluster condensation mechanism, expected under strongly acid conditions.[13] The proportions of $T^J$ and $Q^J$ species present in the hybrid nanocomposites were extracted from the spectra by a peak fitting procedure using Gauss functions to determine the relative peak area of each species. In agreement with the nominal proportions of TEOS to MPTS, the intensity ratio of $Q^J/T^J$ species was found to be approximately 2. The degree of condensation ($C_d$) of the inorganic phase was

 

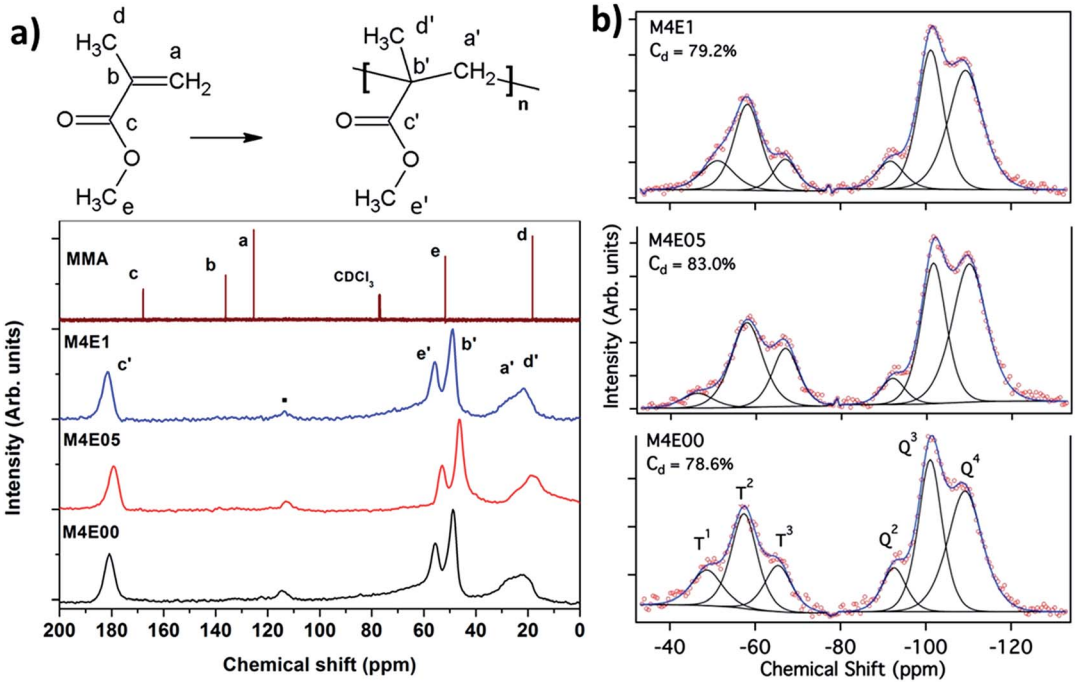


Fig. 1 $^{13}C$ NMR (a) and $^{29}Si$ NMR (b) spectra of PMMA–SS hybrids prepared at EtOH/$H_2O$ molar ratios of 0.0, 0.5 and 1.0.

calculated from the relative proportions of each $T^J$ and $Q^J$ species according to the following equation:

$$C_d = \left[\frac{(T^1 + 2T^2 + 3T^3)}{3} + \frac{(Q^1 + 2Q^2 + 3Q^3 + 4Q^4)}{4}\right] \quad (1)$$

The degrees of condensation extracted from the spectra were for all samples in the range of 78.6 ± 0.5% to 83.0 ± 0.5%. The data revealed the highest $C_d$ value, of about 83%, for the sample prepared at an intermediate EtOH/$H_2O$ ratio (M4E05), indicating the existence of an optimum ethanol proportion, which results in highest connectivity of the inorganic network. As will be shown below, these results are supported by chemical shifts, obtained by XPS, indicating for the M4E05 hybrid the formation densely branched silica cross-linking nodes.

A closer analysis of the NMR spectra showed that the increase of the polycondensation degree, achieved at intermediate ethanol content, is principally caused by the increase of the fully condensed $T^3$ species on the expense of dimeric T1 structures and only to a lower extent by the increase of $Q^4$ species. This will be discussed in the following by correlating NMR data with nanostructural results obtained from SAXS measurements.

SAXS intensity profiles corresponding to PMMA–SS unsupported films prepared at different EtOH/$H_2O$ ratios are displayed in Fig. 2a. The shape of the scattering curves can be classified in two groups of samples: those prepared at intermediate and the others at extreme EtOH/$H_2O$ ratios. For the latter the SAXS pattern exhibits in the low $q$-region a small plateau marking the transition to a Gaussian decay, indicative for the Guinier regime, and an asymptotic linear trend at high $q$-range ($q > 0.7$ nm$^{-1}$) with a slope $-\alpha \sim 1.8$–2.1. Due to the decade range of linearity and to the low slope value, we assume that this regime is associated to the presence of a mass fractal structure with dimensionality $D = -\alpha$.[14] Moreover, the observed Guinier regime implies that the fractal constitutes a dilute set of non-interacting object dispersed in a homogenous matrix. Considering for all samples a volume fraction of inorganic phase of less than 30% the scattering centers can be attributed to the silica–siloxane nano-aggregate embedded in the PMMA matrix.[15] The shift of the plateau to higher $q$-values for the highest EtOH/$H_2O$ ratio indicates a decrease of size of the fractal aggregates.

In contrast, the SAXS curves of samples prepared at intermediate EtOH/$H_2O$ ratios (M4E02 and M4E05) exhibit a discrete maximum that shifts to lower $q$ values with decreasing EtOH amount. As displayed in the linear plot (inset of Fig. 2a), this peak is more evident for the M4E05 sample, while the maximum for M4E02 is at slightly below the minimum $q$ value probed by the SAXS beamline setup. In a previous study this peak has been assigned to an interference effect in the X-ray scattering amplitude produced by the existence of a spatially correlated set of isolated silica–siloxane particles (concentrated solution regime) embedded in homogeneous organic polymeric matrix.[16]

To extract the nanostructural parameters, the same formalism based on the two-electron-density model and the spatial correlation of hard spheres, described by the semi-empirical equation proposed by Beaucage *et al.*,[17] was applied to fit all experimental SAXS curves. The procedure to extract by this model the average interparticle distance, $d$, the packing factor, $k$, the average gyration radius of the siloxane aggregates,

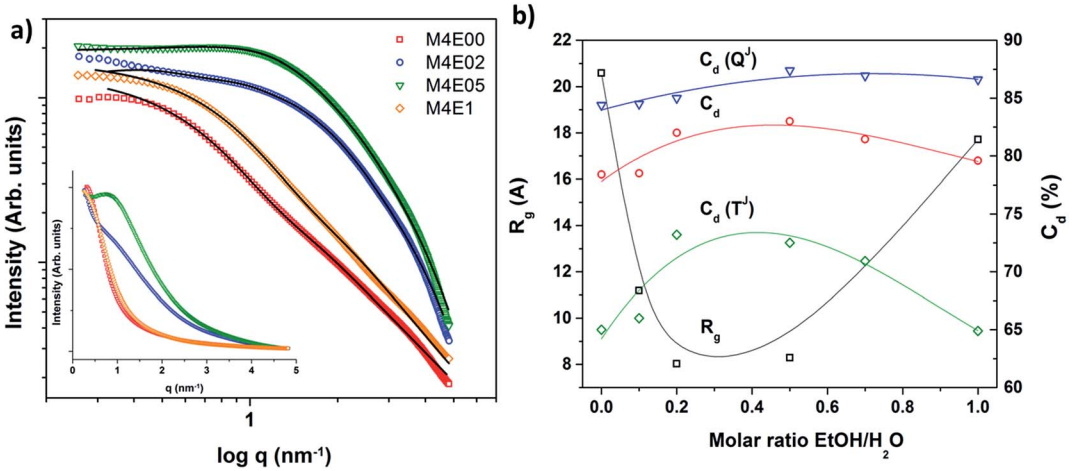


Fig. 2 (a) Fitted SAXS intensity profiles $I(q)$ for PMMA–SS hybrids prepared at different EtOH/$H_2O$ molar ratios (inset: linear scale intensities). (b) Silica–siloxane domain size ($R_g$) and polycondensations degree $C_d$, $C_d(T^J)$ and $C_d(Q^J)$ as a function of EtOH/$H_2O$ molar ratio. The solid curves are guides for the eye. The errors bars are within in the size of the symbols.

$R_g$, and the Porod exponent, $\alpha$, is detailed in a previous study (see ESI†).[18] The best fits of the theoretical model to the experimental SAXS curves are displayed as continuous lines in Fig. 2a.

Among the structural parameters, extracted from the fitting procedure, the average gyration radius is an important value as it is indicative for the size of the scattering centers. The $R_g$ and the polycondensation degree, $C_d$, are plotted in Fig. 2b for hybrids prepared with different EtOH/$H_2O$ ratios. The isolated silica–siloxane particles present in the samples prepared at intermediate EtOH/$H_2O$ ratios show the lowest $R_g$ values (~0.8 nm), being almost three times smaller than those determined for average gyration radius of the silica–siloxane fractal aggregates presents in the M4E00 (2.1 nm) and M4E1 (1.8 nm) samples. Considering the latter hybrids, the similarity of the straight lines slope observed for $q > 0.7$ nm$^{-1}$ suggests that both synthesis conditions lead to the same class of fractal aggregation growth process (Fig. 2a). The relatively low branched open structure, expected for the low fractal dimensionality ($D = -\alpha \sim 2$) is in agreement with NMR analysis, which shows similar low $C_d$ values for both hybrid materials. However, the slope values determined from the fitting procedure indicate a significant decrease of $\alpha$ from −1.8 to −2.1 when EtOH/$H_2O$ ratio increases from 0.0 to 1.0. The slope of −1.8 corresponds to the mass fractal dimension ($D = 1.8$) of structures formed by the diffusion limited cluster–cluster growth (DLCC), while $D = 2.1$ is expected for reaction limited cluster–cluster growth (RLCC).[19] This change from DLCC to RLCC is consistent with the low solubility of water in TEOS, which limited the condensation reaction by the diffusion of water molecule through the non polar medium of M4E00 sample. For samples with intermediate ethanol content the observed correlation peak suggests the formation of a densely cross-linked hybrid network, consisting of compact silica–siloxane nodes.

For a better understanding of the effect of ethanol on the formation of the inorganic phase, we correlated the ethanol content dependence of silica domains size ($R_g$), calculated from the SAXS data, with the NMR polycondensation degree of $T^J$ and $Q^J$ species. To calculate $C_d(T^J)$ and $C_d(Q^J)$ the relative sub-peak areas of the $T^J$ as well as $Q^J$ spectra were renormalized to 100%. Fig. 2b shows that the increase of the polycondensation degree for intermediate EtOH/$H_2O$ ratios is mainly related to the connectivity increase of $T^J$ species, the polycondensation product of MPTS. Consequently, the coincidence of the minimum of $R_g$ with the maximum of $C_d(T^J)$ reflects the enhanced polycondensation of hydrolyzed alkoxide groups of TEOS with those belonging to the MPTS coupling agent. The average gyration radii of M4E02 and M4E05 samples are larger than those expected for the most stable polyhedral structure, which is the cube-like octamers $Q_8^3$ ($R_g \approx 0.22$ nm).[19] In fact the relative abundance of $T^J$ species at an average radius of about 0.8 nm, found for these samples, can be explained by the presence of building block ($Q_8^{3-4}T_3^3$ or $Q_8^{3-4}T_4^2$) formed by the addition of the $Q_8^3$ cube to the surface of cyclic $T^2$ species ($T_3^2$ trimers or $T_4^2$ tetramers).[19] Thus the enhanced connectivity of the hybrid network, consisting of dense silica–siloxane crosslink nodes bridged by short polymeric chains explains the improved thermal stability of samples prepared at intermediate EtOH/$H_2O$ ratios (ESI, Fig. S1†). The short distance between silica nodes ($d = 4.6$ nm), found from the fitting procedure, which is less than three times the node size ($2R_g = 1.6$ nm), coupled with the low packing factor, $k = 0.3$, suggests that hybrid network of sample M4E05 is formed by relatively low number density of compact silica–siloxane crosslinks, densely interconnected by PMMA chains.

The quantitative XPS analysis confirmed the formation of PMMA–SS hybrids with a fixed organic to inorganic phase ratio, in good agreement with the nominal MMA : MPTS : TEOS proportion of 8 : 1 : 2, corresponding to 58.7 at% carbon, 34.8 at% oxygen and 6.5 at% silicon. The influence of the EtOH/$H_2O$ ratio on chemical bonding structure of the coated samples was investigated by the deconvolution of the XPS C 1s, O 1s and Si 2p

 

spectra, shown in Fig. 3a. The scheme, displayed in Fig. 3b, illustrates the hybrid structure formed from MMA, MPTS and TEOS precursors. The following four components of the C 1s correspond to different chemical environments of carbon: the hydrocarbon sub-peak (C–C) at 284.8 eV, the C–COO sub-peak at 285.6 eV, corresponding to second neighbor interaction chemical shift of the carbon linked to the adjacent ester group, the ether group component (C–O) centered at 286.4 eV and the ester group (O–C=O) at 288.8 eV.[20] The constant intensity ratio of these components (C–C : C–COO : C–O : O–C=O = 2.5 : 1 : 1 : 1), observed for all samples, reflects the fixed proportion of carbon atoms in the respective bonding states given by the fixed MMA to MPTS ratio of 8. It should be noted that the binding energy reference was fixed on the well known position (288.8 eV) of the ester sub-peak (Fig. 3a). The fitted O 1s spectra show the three bonding environments of oxygen: the main sub-peak at about 532.8 eV is related to O–Si bonds and the other two to oxygen atoms of the ester group, already identified in the C 1s spectra, located at 532.1 eV (O–C=O) and 533.8 eV (O–C=O).[18] The intensity ratio of these sub-peaks of O–Si : O–C=O : O–C=O = 1.2 : 1 : 1, observed for all samples, is in agreement with the fixed proportion between MMA, MPTS and TEOS. Finally, the single component of the Si 2p spectra is related to Si–O bonds.

Analyzing in more detail the fitted O 1s and Si 2p spectra upon variation of the EtOH/$H_2O$ ratio, a clear shift of the position of Si–O (Si 2p) and O–Si (O 1s) sub-peaks can be observed. Plotting now for all samples the binding energy of the Si 2p peak *vs.* the O–Si component (O 1s), a linear relationship was obtained (Fig. 4a). The shift to higher binding energies indicates an increasing covalent character of the O–Si bond paired with an increasing oxidation state of silicon, moving to a more stoichiometric silica phase (103.5 eV).[20] It is interesting to note, that hybrid samples prepared at an intermediate EtOH/$H_2O$ ratio of 0.5 show the highest binding energies, indicative for a high connectivity of the inorganic phase, as evidenced by NMR. This hypothesis was confirmed by a correlation of XPS and NMR data, showing a linear dependence between the Si–O sub-peak position and the polycondensation degree ($C_d$) (Fig. 4b). This interesting result shows first that XPS and NMR chemical shifts scale linearly and second that it is possible to determine the degree of connectivity of inorganic phases more rapidly (10 min) from XPS spectra than $^{29}$Si NMR measurements, taking about 3 days at the used conditions.

Additional information on the overall connectivity of the hybrid network was obtained from thermogravimetric measurements (TG, ESI, Fig. S1†). TG and DTG (first derivative) results showed that the material starts to degrade at about 150 °C and decomposes completely at ~400 °C by random scissions of the polymer chains.[21,22] It is worth pointing out that hybrids prepared at intermediate EtOH/$H_2O$ ratios exhibit a superior thermal stability by shifting the begin of degradation to higher temperatures (~50 °C) and by suppressing the rate of intermediate degradation events, associated with the rupture of the head-to-head segments (~250 °C) and to unsaturated chain ends (~310 °C).[21,22] These findings suggest a substantial increase of the thermal stability of hybrids formed at

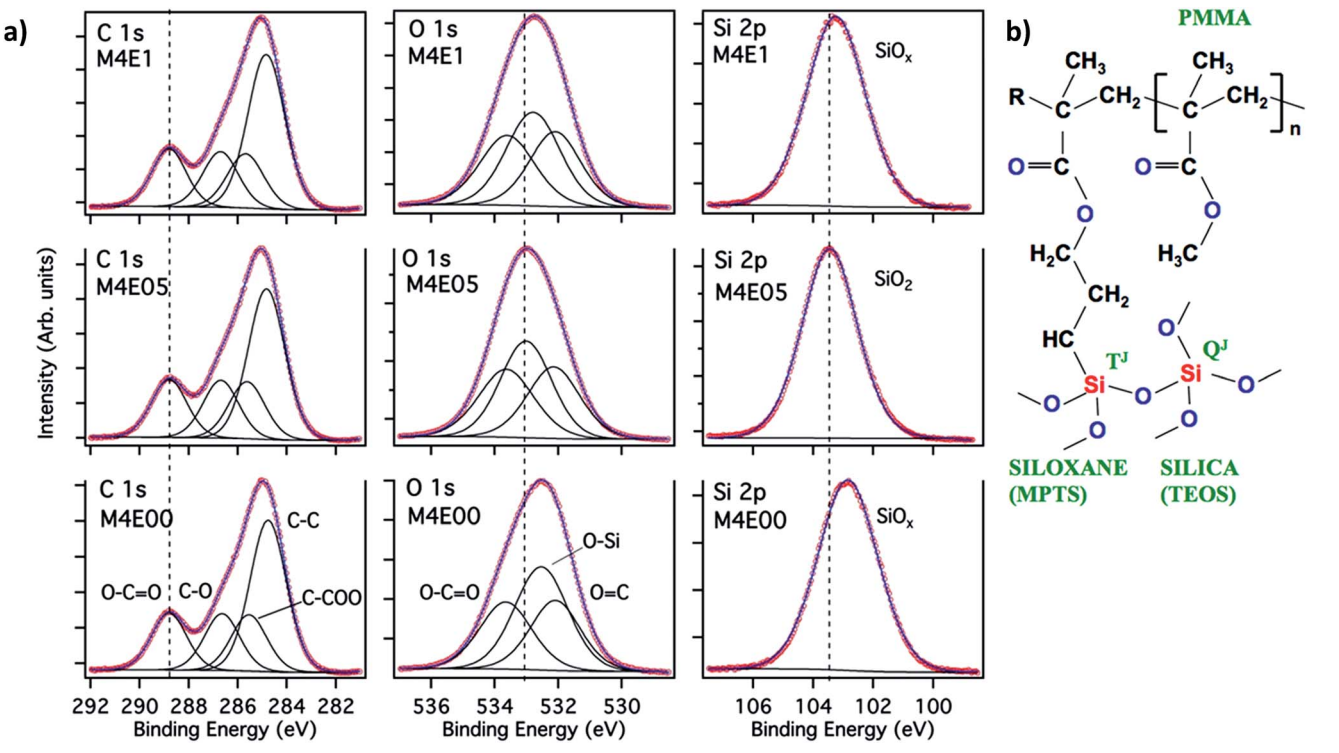


Fig. 3 (a) Fitted XPS, C 1s, O1s and Si 2p spectra of PMMA–SS obtained for three different EtOH/$H_2O$ molar ratios: 0, 0.5 and 1.0. (b) Scheme illustrating the hybrid structure formed from MMA, MPTS and TEOS precursors.

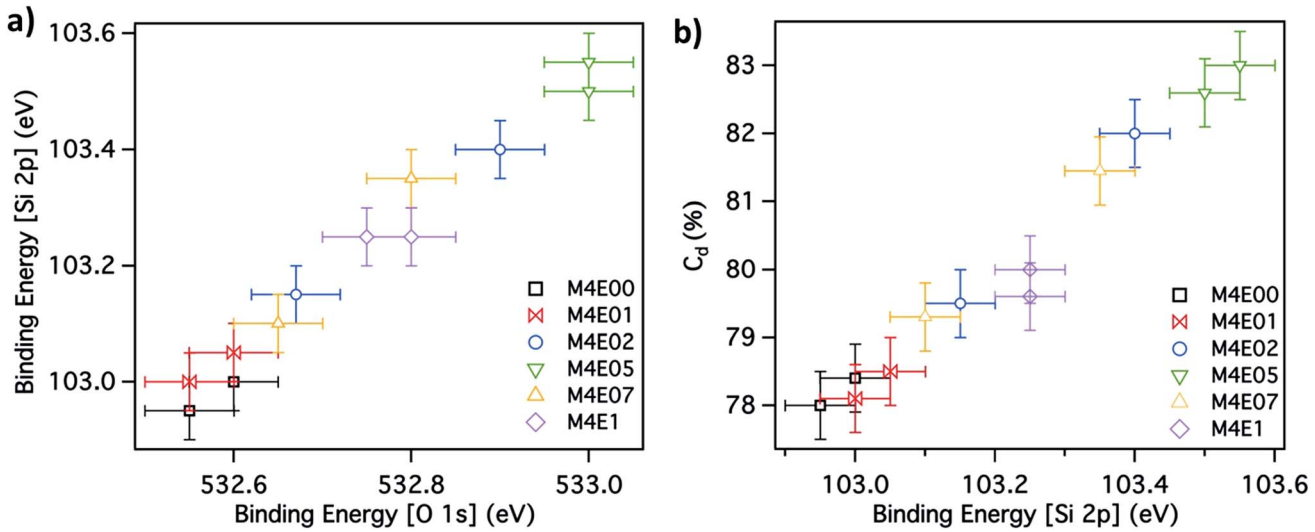


Fig. 4 EtOH/$H_2O$ ratio dependence of (a) XPS binding energies of the Si–O sub-peak (Si 2p) *vs.* the O–Si component (O 1s) and (b) poly-condensation degree $C_d$ of NMR data *vs.* the XPS binding energy of the Si–O sub-peak (Si 2p).

intermediate EtOH/$H_2O$ ratios, in agreement with results obtained from $^{13}C$ and $^{29}Si$ NMR experiments.

Considering the structural data, the correlation of NMR, SAXS, XPS and TG/DTG results provided clear evidence that hybrids prepared at intermediate EtOH/$H_2O$ ratios form a structure of ramified inorganic domains interconnected covalently by a dense network of the short polymeric chains. Consequently, it was expected that these structural properties might lead to a substantial improvement of the mechanical and anticorrosive properties of the material.

### Mechanical properties

All hybrid films were transparent, defect free and presented a very smooth featureless surface (RMS roughness ≈ 0.5 nm), indicating the formation of a dense and homogeneous layer (ESI, Fig. S2a and S2b†). Depending on the ethanol to $H_2O$ ratio, the film thickness varied in the range of 1.5–2.0 μm.

The tensile pull-off force of detaching, determined by the ASTM D4541 method, was for all coatings in the range of 3.6–4.0 MPa, indicating a very good adhesion of the film to the substrate. This is a consequence of the covalent interaction between the steel substrate and the silanol groups of the inorganic part of the hybrid. The results of this method are in agreement with complementary results, determined by scratch test measurements, which provided the friction coefficient and critical loads for plastic deformation and cracking. No film delamination was observed on the 1 mm track with loads up to 100 mN (Fig. 5a).

Fig. 5a displays a representative scratch test data set of the coated M4E05 sample, including the track dependence of the tangential force response ($F_t$), penetration depth ($P_d$) and the residual depth ($R_d$). The $R_d$ value of about 2 μm is comparable with the thickness for the coating. The critical loads for beginning crack formation (Fig. 5b) and the appearance of first large cracks (Fig. 5c), determined from optical microscopy images of the scratch track, were similar for all coated samples (ESI, Table S1†). The friction coefficient was in the range of 0.5–0.7, similar to that of carbon steel (0.6). The absence of film delamination confirmed the results of ASTM D4541 adhesion tests, showing an excellent adhesion of the hybrid coatings to the metallic surface.

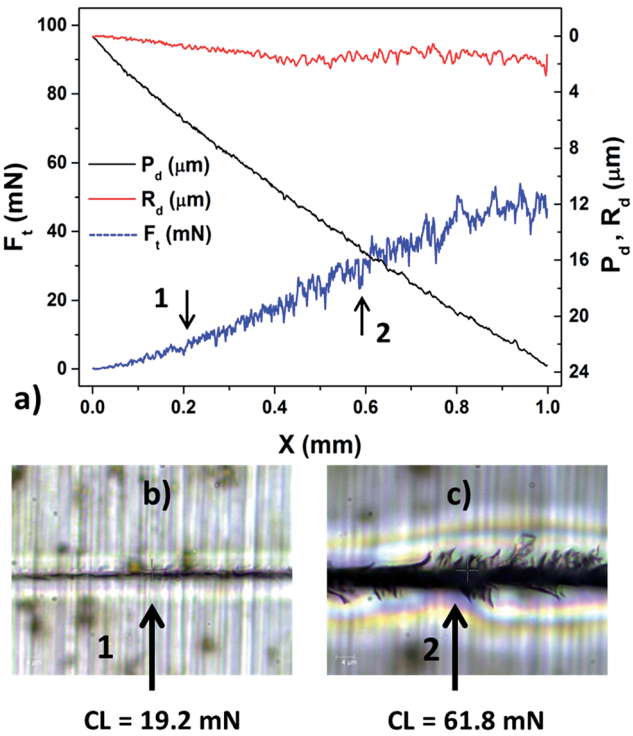


Fig. 5 Scratch results of coated steel samples prepared at EtOH/$H_2O$ = 0.5: (a) track distance dependence of the tangential force response ($F_t$), penetration depth ($P_d$) and the residual depth ($R_d$); (b) and (c) optical microscopy image of the scratch track, indicating the critical loads for the begin of crack formation (1) and the begin of formation of larger cracks (2), respectively.

 

The nanoindentation experiments have shown for all samples that the coating hardness was in the range between 311.0 ± 5.0 MPa (M4E00) and 321.3 ± 5.6 MPa (M4E1), values about 30% higher than that of PMMA (220–260 MPa), however significantly lower than amorphous $SiO_2$ (7–9 GPa). The Young modulus was in the range between 5.4 ± 0.1 GPa (M4E00) and 6.3 ± 0.1 GPa (M4E1), somewhat higher than pure PMMA (1.8–3.1 GPa), but considerable lower than the elastic modulus of silica (75 GPa). These values are in agreement with those expected for a PMMA–SS hybrid that contains about 70% of polymethacrylate groups.

## Corrosion analysis

The corrosion protection efficiency of hybrid coatings, prepared using different EtOH/$H_2O$ ratios, was evaluated using electrochemical impedance spectroscopy curves, recorded after 1 day of immersion in saline and saline/acidic environment as well as after long-term exposure to both solutions. Fig. 6 shows the complex plane impedance and the Bode plots (log|$Z$| and $\theta$ *vs.* log $f$) for bare carbon steel, M4E00, M4E02, M4E05, M4E07 and M4E1 hybrid coatings. Compared to the bare steel substrate, the coated samples show about 5 orders of magnitude higher impedance modulus, reaching for the M4E07 sample almost 5 GΩ cm$^2$ in saline environment (Fig. 6b). This value is about one magnitude higher than that reported recently for similar PMMA–SS hybrids.[5] It is interesting to note that all coated samples showed a phase angle dependence (Fig. 6c) with $\theta < -80°$ extending over 4 orders of magnitude, suggesting a capacitive behavior with strongly blocking character. The form of the phase angle curves hints on the presence of two time constants, one in the high frequency range (~1 kHz), and a second in the low frequency (~0.5 Hz). It is important to stress that this electrochemical performance, featuring elevated impedance modulus and almost pure capacitive behavior over a range of about 4 orders of magnitude approaches the behavior of high performance paints, however achieved with about 100 times smaller thickness.

Despite of the excellent barrier properties observed after one day of exposure, the crucial point for applicability of a protective coating is its long-term stability in the aggressive environments. Even for thick, homogeneous and highly hydrophobic coatings, like paints and chromates, a long-term corrosion cannot be completely prevented, principally due intrinsic structural defects and low levels of residual porosity. Regarding the protective organic–inorganic hybrid sol–gel coatings a recent review concludes that after a detailed analysis of a large set of publications no studies on the time dependence of the barrier properties were found.[23] However, the following results

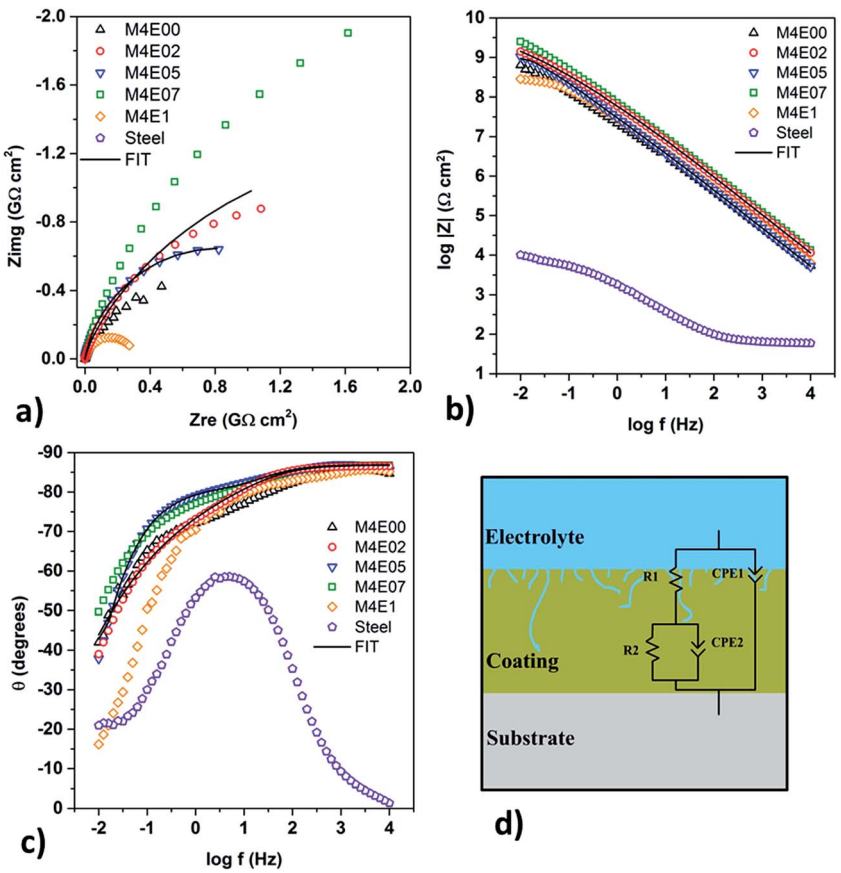


Fig. 6 Complex plane impedance (a), impedance modulus (b) and phase angle plots (c) of bare carbon steel and PMMA–SS hybrid coated steel prepared at EtOH/$H_2O$ ratios in the range of 0.0–1.0, after 1 day exposure to unstirred and naturally aerated 3.5% NaCl. (d) Schematic representation of substrate/coating/electrolyte system and the equivalent circuit used to fit the EIS data.

obtained for PMMA–SS hybrids show that considerable durability and thus a significant increase of product lifetime, which is of extreme economical importance, can be achieved using a very thin, low-cost and environmentally compliant organic–inorganic coating system. Fig. 7 displays the time dependence of the hybrid coating M4E02, presenting the highest stability in saline and acidic NaCl solution. The Nyquist and Bode plots show only a very small decrease of the barrier properties, after more than 6 month of exposure to saline solution (NaCl 3.5%) and more than 3 months in the acidic NaCl medium. Similar corrosion protection efficiency was observed for the M4E05 coating (>2 months in saline medium), while all other films resisted for several weeks the aggressive media. The most relevant fact is that this performance was achieved without addition of corrosion inhibitors for a coating thickness of only ~2 μm. Comparable corrosion protection efficiency in saline medium, presenting coating resistance of up to $2 \times 10^{10}$ Ω cm$^2$ over 6 months were reported for a silicon polyester coated galvanized steel system, though for a film thickness of 25 μm.[24] In terms of long-term stability, a durability of more than 10 months in 3.5% saline solution was recently achieved for PMMA–SS coatings doped with cerium(IV), which was used as corrosion inhibitor.[25]

To quantify the electrochemical parameters of the processes taking place during the long-term exposure, the equivalent circuit, shown in Fig. 6d, was used to fit the experimental data for the M4E02 and M4E05 samples. According to this circuit, the EIS curves were fitted using two time constants: $R_1$ and $CPE_1$ refer to the high frequency resistance and constant phase element of the upper film layer (small initial paths), as expected for the electrolyte uptake process, while $R_2$ and $CPE_2$ are related to the low frequency resistive and capacitive response of the layer close to the coating/steel interface.[4,26] The derived model parameters are summarized in Table S2 of the ESI.† Both samples (M4E02 and M4E05) present high values of the $R_1$ and $R_2$ (>$10^7$ Ω cm$^2$), characteristic for a high-performance corrosion barrier. The time dependence of the circuit parameters shows for the M4E02 coating an almost unchanged $R_1$ value of the uptake zone and a slight decrease of $R_2$, related to the migration of the electrolyte uptake towards the coating/steel interface. In contrast to the corrosion process in saline solution, where the drop of $R_2$ takes place after two weeks of exposure, the diffusion process is continuous in the case of contact with the saline/acidic environment (Fig. 7b2).

According to the electrochemical tests, the performance against corrosion in neutral saline and saline/acidic media was established in the following order: M4E02 > M4E05 ≈ M4E07 > M4E00 > M4E1 ≫ steel. This result can be related to the higher network connectivity in the intermediate range of the EtOH/$H_2O$ ratio, as suggested by the correlation of NMR, SAXS and XPS data. The covalent interaction on the molecular scale of a highly cross-linked inorganic phase, formed by sub-nanometric silica particles, with the highly polymerized organic moieties leads to a hybrid nanocomposite material with elevated overall connectivity, responsible for the excellent

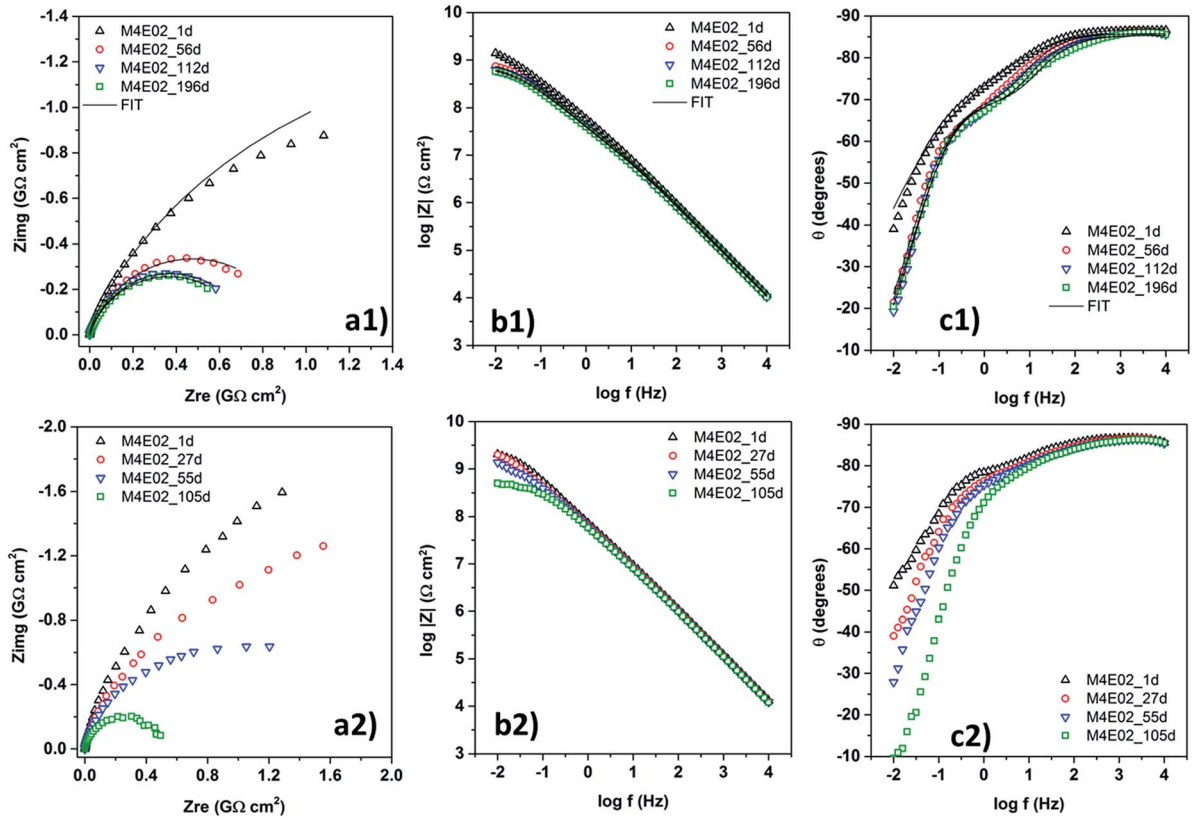


Fig. 7 Complex plane impedance (a), impedance modulus (b), and phase angle (c) plots of the M4E02 sample after exposure of up to 196 days (1) exposure in naturally aerated 3.5% NaCl, and up to 105 days (2) in 0.05 mol L$^{-1}$ NaCl + 0.05 mol L$^{-1}$ $H_2SO_4$ solution.

 

thermal and barrier properties of the coatings. The high corrosion resistance (>1 GΩ), the broad capacitive phase angle dependence and the excellent long-term stability, principally in neutral chloride medium, highlight the exceptional performance of these coatings for wet corrosion protection.

## Conclusions

Smooth, defect-free and optically transparent PMMA–siloxane–silica hybrid coatings, prepared by the sol–gel route at different ethanol to water ratios (0.0–1.0), were deposited onto carbon steel from a sol prepared by acid-catalyzed hydrolytic polycondensation of TEOS and MPTS and radical polymerization of MMA. NMR results have shown a complete polymerization of the organic phase and evidenced a high polycondensation degree of the inorganic silica–siloxane nodes of up to 83% for samples prepared at intermediate $EtOH/H_2O$ ratios. SAXS results revealed that the high connectivity of the inorganic network in this ethanol concentration regime is induced by the hydrolytic polycondensation of reticulated sub-nanometric silica domains densely interconnected by short PMMA chains. The consequence is an increase of the overall network connectivity, leading to a substantial improvement of the mechanical, thermal and electrochemical properties of the material. A correlation between the XPS and NMR data was found, showing a linear relationship between the XPS binding energies of the Si–O sub-peak of the Si 2p and O 1s spectra and the NMR polycondensation degree, confirming the formation of a highly branched silica–siloxane nodes reaching almost the silica stoichiometry. These dense and homogenous coatings with a thickness of only ~2 μm have an elevated adhesion to metallic substrates and provide excellent barrier properties with elevated impedance of up to $5 \times 10^9\ \Omega\ cm^2$ and a very good durability of more than 6 months in contact with neutral saline and 3 months in acidic NaCl solution. Based on these results, sol–gel PMMA–SS hybrids can be considered as very promising candidates for environmentally friendly substitutes of chromate-based protective coatings.

## Acknowledgements

We are grateful to FAPESP, CNPq and CAPES for the financial support and to the National Laboratory of Synchrotron Light Source (LNLS) for the use of SAXS facilities.

## Notes and references

1 C. Sanchez, L. Rozes, F. Ribot, C. Laberty-Robert, D. Grosso, C. Sassoye, C. Boissiere and L. Nicole, *C. R. Chim.*, 2010, **13**, 3–39.
2 E. F. Molina, L. Marcal, H. W. P. D. Carvalho, E. J. Nassar and K. J. Ciuffi, *Polym. Chem.*, 2013, **4**, 1575–1582.
3 C. Sanchez, G. J. D. A. A. Soler-Illia, F. Ribot and D. Grosso, *C. R. Chim.*, 2003, **6**, 1131–1151.
4 V. H. V. Sarmento, M. G. Schiavetto, P. Hammer, A. V. Benedetti, C. S. Fugivara, P. H. Suegama, S. H. Pulcinelli and C. V. Santilli, *Surf. Coat. Technol.*, 2010, **204**, 2689–2701.
5 P. Hammer, F. C. dos Santos, B. M. Cerrutti, S. H. Pulcinelli and C. V. Santilli, *J. Sol-Gel Sci. Technol.*, 2012, **63**, 266–274.
6 P. Hammer, M. G. Schiavetto, F. C. dos Santos, A. V. Benedetti, S. H. Pulcinelli and C. V. Santilli, *J. Non-Cryst. Solids*, 2010, **356**, 2606–2612.
7 S. Bhattacharyya, M. B. Das and S. Sarkar, *Eng. Failure Anal.*, 2008, **15**, 711–722.
8 D. A. López, N. C. Rosero-Navarro, J. Ballarre, A. Durán, M. Aparicio and S. CERÉ, *Surf. Coat. Technol.*, 2008, **202**, 2194–2201.
9 S. Zheng and J. Li, *J. Sol-Gel Sci. Technol.*, 2010, **54**, 174–187.
10 C. V. Santilli, V. H. V. Sarmento, K. Dahmouche, S. H. Pulcinelli and A. F. Craievich, *J. Phys. Chem. C*, 2009, **113**, 14708–14714.
11 L. Delattre, C. Dupuy and F. Babonneau, *J. Sol-Gel Sci. Technol.*, 1994, **2**, 185–188.
12 R. Avolio, G. Gentile, M. Avella, D. Capitani and M. E. Errico, *J. Polym. Sci., Part A: Polym. Chem.*, 2010, **48**, 5618–5629.
13 K. Saravanamuttu, X. M. Du, S. I. Najafi and M. P. Andrews, *Can. J. Chem.*, 1998, **76**, 1717–1729.
14 A. Guinier, *Theorie et Technique de la Radiocristallographie. Dunod*, Paris, FR, 1956.
15 V. H. V. Sarmento, K. Dahmouche, C. V. Santilli, S. H. Pulcinelli and A. F. Craievich, *J. Appl. Crystallogr.*, 2003, **36**, 473–477.
16 C. J. T. Landry, B. K. Coltrain, J. A. Wesson, N. Zumbulyadis and J. L. Lippert, *Polymer*, 1992, **33**, 1496–1506.
17 G. Beaucage, T. A. Ulibarri, E. P. Black and D. W. Schaefer, in *Hybrid Organic-Inorganic Composites*, ed. J. E. Mark, C. Y.-C. Lee and P. A. Bianconi, American Chemical Society, Washington DC, USA, 1995, pp. 97–111.
18 M. C. Gonçalves, N. J. O. Silva, V. de Zea Bermudez, R. A. Sá Ferreira, L. D. Carlos, K. Dahmouche, C. V. Santilli, D. Ostrovskii, I. C. Correia Vilela and A. F. Craievich, *J. Phys. Chem. B*, 2005, **109**, 20093–20104.
19 C. J. Brinker and G. W. Scherer, *Sol-Gel Science, the Physics and Chemistry of Sol-Gel Processing*, Academic Press, New York, USA, 1990.
20 A. V. Naumkin, A. Kraut-Vass, S. W. Gaarenstroom and C. J. Powell, *NIST X-Ray Photoelctron Spectroscopy Database*, Standard Reference Database 20, 2012, vol. 4.1, http://www.srdata.nist.gov/XPS/.
21 T. Hirata, T. Kashiwagi and J. E. Brown, *Macromolecules*, 1985, **18**, 1410–1418.
22 H. W. P. Carvalho, A. F. Suzana, C. V. Santilli and S. H. Pulcinelli, *Polym. Eng. Sci.*, 2013, **53**, 1253–1261.
23 R. B. Figueira, C. J. R. Silva and E. V. Pereira, *J. Coat. Technol. Res.*, 2015, **12**, 1–35.
24 V. Lavaert, M. de Cock, M. Moors and E. Wettinck, *Prog. Org. Coat.*, 2000, **38**, 213–221.
25 S. V. Harb, F. C. dos Santos, B. L. Caetano, S. H. Pulcinelli, C. V. Santilli and P. Hammer, *RSC Adv.*, 2015, **5**, 15414–15424.
26 D. Loveday, P. Peterson and B. Rodgers, *J. Coat. Technol.*, 2004, 88–93.